Method of Moments Evaluation of the Two-Dimensional Quasi-Crystalline Approximation

Paul R. Siqueira and Kamal Sarabandi, *Senior Member, IEEE*

Abstract— **The purpose of this paper is to characterize the accuracy of the quasi-crystalline approximation and other associated methods of determining effective permittivity for two-dimensional (2-D) random media. A numerical method based on the method of moments is used as a gauge for comparison with the theoretical methods. After deriving the 2-D quasi-crystalline approximation and presenting the numerical method, the behavior of the effective permittivity is analyzed for a range of particle sizes, volume fractions and dielectric losses. From this analysis, regions of validity for the theoretical methods are determined. An investigation is also given which explores the effect of particle arrangement methods on the pair distribution function which, in turn, is shown to have a significant effect on the imaginary component of the effective permittivity.**

I. Introduction

In remote sensing, the propagation of electromagnetic fields through random media is often of concern. We may wish to characterize the effects of clouds or water droplets along the line of sight between an airplane and a radar installation, or we may be interested in using radars to probe the random medium itself, such as in determining snow depth and particle size. In all of these problems it is necessary to predict the propagation constant in the "random" medium. When the observing wavelength is much larger than a typical dimension of the inhomogeneities making up the medium, no significant scattering occurs, and we can generally approximate the medium as being electrically homogeneous. Methods which utilize this approximation are termed mixing formulas, formulas that determine the constant of propagation by combining the effect of small-scale inhomogeneities through a simple algebraic equation. The most common of these formulas is the Polder-Van Santen (PVS) mixing formula [1956]. When the observing wavelength and the inhomogeneities are similar in size, we must take into account scattering from individual inhomogeneities. This is typically done using a field approach based on Maxwell's equations, the most common of which are the effective field approximation (EFA—also known as Foldy's approximation) for low-density media and the quasi-crystalline approximation (QCA) or the quasi-crystalline approximation with coherent potential (QCA-CP) for higher density media.

All of the aforementioned theoretical methods for determining the effective propagation constant make approximations in their formulation to make the theory tractable. As the theory becomes more complex, it becomes more difficult to test the region of validity of these approximations and to test the effects of the approximation employed in the method. The validity of these models may be checked in one of three ways: 1) theoretically, 2) experimentally, or 3) numerically.

The field approaches may be checked via theoretical methods by taking the limiting case of the approach and comparing it to more standard, well-accepted, theoretical results. Common limiting cases use either zero or unity volume fraction, or examine the problem in the low- or high-frequency limits. While these limiting cases perform the important task of giving a shortcut to provide a sanity check for a more complicated theory, they may often zero-out important terms in the field-approach theory. Thus, instead of testing the new theory, we find ourselves simply checking that the coefficients for zero- or first-order terms have been derived correctly.

The second method of checking the theories is to back them up with experiments. This can be the true test of any theory because it is the measurement in the end for which the theory is to be applied. Experiments, however, must be designed carefully so as to minimize experimental errors and to accurately characterize physical parameters about the random medium. For the application of the QCA and QCA-CP it is necessary to determine the pair distribution function of particle positions, a function that is very difficult to measure experimentally. Alternatively, the pair distribution function can be specified beforehand and particle positions in a controlled experiment can be determined by a computer, as was done by Mandt *et al.* [4]. Finally, an experiment may be difficult and time consuming to perform over a controlled range of variables (such as volume fraction and particle size). For this reason, while an experiment may be used to test validity of a theory for a particular application, it is much more difficult to make generalizations based on this experiment.

The third method of analyzing theoretical field approaches of determining the constant of propagation is to do so numerically. This method removes the need for theoretical simplification or the problem of experimental uncertainty by solving for the electromagnetic fields directly. Numerical methods may be difficult to implement due to computational limitations or our inability to model the problem accurately. This problem has been partially addressed using a T-matrix approach in three dimensions [3], [12]. In this work, the incoherent scattered field is calculated and related to the extinction coefficient by a diffuse boundary approximation [Sarabandi and Siqueira, *in review*], the result of which is

Manuscript received June 2, 1995; revised December 27, 1995. This work was supported by ARO Grant DAAH04–93–G-0156.

The authors are with the Radiation Laboratory, Electrical Engineering and Computer Science Department, University of Michigan, Ann Arbor, MI 48109 USA.

Publisher Item Identifier S 0018-926X(96)04751-5.

0018–926X/96$05.00 © 1996 IEEE

compared to the theoretical calculations of QCA and QCA-CP. Good agreement is shown for Rayleigh sized ($ka = 0.2$) lossless particles with volume fractions extending up to 25%, but this application is limited by the numerical solution's reliance on incoherent field calculations. Furthermore, the incoherent approach described in these papers supplies only the extinction coefficient and does not address the issue of determining both the real and imaginary components of complex permittivity. Thus, it has been necessary to develop a method which addresses the effective permittivity problem fully.

In answer to this need, a method has been developed for determining the effective permittivity of a random medium using a coherent approach [Sarabandi and Siqueira, *in review*]. In two dimensions, this approach has been tested and verified over a wide range of volume fractions (ranging from 0–80%), varying discontinuity size ($ka = 0.2$ to $ka = 0.5$) and absorption loss. Given the flexibility and generality of the coherent numerical method, it may be used as a tool to explore two-dimensional (2-D) versions of the field theories and to provide guidance for the three-dimensional (3-D) problem.

This paper addresses the 2-D quasi-crystalline approximation and its dependence on the pair distribution function. Section II of this paper presents a derivation of 2-D QCA based on the 3-D version found in Tsang *et al.* [13] and gives the related results of 2-D EFA. Section III discusses different methods of obtaining particle arrangements and their associated pair distribution function. In the fourth section, we review the coherent method for numerically determining the effective permittivity of a 2-D random medium, and present 2-D theoretical results for the Polder-Van Santen mixing formula. In the fifth section of this paper, we compare the results of our numerical analysis with that of QCA.

II. Two-Dimensional Quasi-Crystalline Approximation

The 2-D derivation of QCA follows closely the work of Tsang *et al.* [13], where we begin with the multiple scattering equation for plane-wave incidence using the T-matrix approach. Consider N cylinders, whose centers are denoted by $\bar{r}_l$ $(l = 1, \cdots, N)$, randomly distributed over an area A. Expanding the fields in terms of cylindrical basis functions, it can be shown that [13, p. 454]

$$\bar{\mathbf{w}}^{(l)} = \sum_{\substack{j=1 \\ j\neq l}}^{N} \bar{\bar{\sigma}}(k\overline{r_l r_j})\bar{\bar{\mathbf{T}}}^{(j)}\bar{\mathbf{w}}^{(j)} + e^{i\bar{k}_i\cdot\bar{r}_l}\bar{\mathbf{a}}_{\text{inc}} \tag{1}$$

where $\bar{\mathbf{w}}^{(l)}$ is the vector of exciting field coefficients for the lth particle, $\bar{\mathbf{a}}_{\text{inc}}$ is the vector of coefficients for the incident field, $\bar{\bar{\sigma}}(k\overline{r_l r_j})$ is the translation matrix from a coordinate system centered on the jth particle to one centered on the lth particle, and $\bar{\bar{\mathbf{T}}}^{(j)}$ is the transition matrix which translates the exciting field of the jth particle into the scattered field from the jth particle. The basis functions for the field expansions are the cylindrical functions [1], $\psi_n = H_n^{(1)}(k\bar{r}_>)e^{\text{in}\phi}$ and $\text{Rg}\,\psi_n = J_n(k\bar{r}_<)e^{\text{in}\phi}$, where $\bar{r}_> = \text{larger}(\bar{r}, \bar{r}')$ and $\bar{r}_< = \text{lesser}(\bar{r}, \bar{r}')$ when $\bar{r}$ is the point of observation and $\bar{r}'$ is the source point. The incident field

$$\Phi_{\text{inc}}(\bar{r}) = \sum_{n=0}^{\infty} \bar{\mathbf{a}}_{\text{inc}}\text{Rg}\,\psi_n(k\bar{r}) \tag{2}$$

may represent either E_z (TM polarization) or H_z (TE polarization). By determining the expected value of (1) with respect to the lth particle, we arrive at

$$E_l\left[\bar{\mathbf{w}}^{(l)}\right] = \sum_{\substack{j=1 \\ j\neq l}}^{N} E_l\left[\,\bar{\bar{\sigma}}\,(k\overline{r_l r_j})\bar{\bar{\mathbf{T}}}^{(j)}E_{jl}\left[\bar{\mathbf{w}}^{(j)}\right]\right] + e^{i\bar{k}_i\cdot\bar{r}_l}\bar{\mathbf{a}}_{\text{inc}}. \tag{3}$$

Under the conditions that the number of particles are large and particle density is not very high, we make the approximation fundamental to QCA that $E_{jl}[\bar{\mathbf{w}}^{(j)}] \approx E_j[\bar{\mathbf{w}}^{(j)}] = \bar{\mathbf{w}}(\bar{r}_j)$ whereby, (3) becomes

$$\bar{\mathbf{w}}(\bar{r}_l) = (N-1)\int_A \bar{\bar{\sigma}}(k\overline{r_l r_j})\bar{\bar{\mathbf{T}}}^{(j)}\bar{\mathbf{w}}(\bar{r}_j)p(\bar{r}_j \mid \bar{r}_l)d\bar{r}_j + e^{i\bar{k}_i\cdot\bar{r}_l}\bar{\mathbf{a}}_{\text{inc}}. \tag{4}$$

If we normalize the conditional probability $p(\bar{r}_j \mid \bar{r}_l)$ to the area, A, we have the pair distribution function, $g(\bar{r})$ such that $p(\bar{r}_j \mid \bar{r}_l) = \frac{1}{A}g(\bar{r}_j \mid \bar{r}_l)$ which has the asymptotic property of approaching unity when $\bar{r}_j - \bar{r}_l$ is large. For a large system of particles, the fraction $\frac{N-1}{A}$ is approximately the particle density, n_0. Letting A be the positive half-space $x_j > 0$ [13, p. 491]

$$\bar{\mathbf{w}}(\bar{r}_l) = n_0\int_{x_j>0} g(\bar{r}_j \mid \bar{r}_l)\bar{\bar{\sigma}}(k\overline{r_l r_j})\bar{\bar{\mathbf{T}}}^{(j)}\bar{\mathbf{w}}(\bar{r}_j)d\bar{r}_j + e^{i\bar{k}_i\cdot\bar{r}_l}\bar{\mathbf{a}}_{\text{inc}}. \tag{5}$$

To evaluate the integral in (5) we use a trial solution for $\bar{\mathbf{w}}(\bar{r}_l) = \bar{\mathbf{a}}_E e^{i\kappa x_l}$ such that it expresses a field traveling in a medium with effective constant of propagation, κ. After substituting the trial solution in (5) and making a simple coordinate transform ($\overline{r_j r_l} = \bar{r}_j - \bar{r}_l = \bar{r}$), the integral in (5) becomes

$$\begin{aligned}\bar{\bar{\mathbf{s}}} &= n_0 e^{i\kappa x_l}\int_S g(\bar{r})\bar{\bar{\sigma}}(k\bar{r})e^{i\kappa x}d\bar{r}\,\bar{\bar{\mathbf{T}}}\bar{\mathbf{a}}_E \\ &= n_0 e^{i\kappa x_l}\left(\int_S \bar{\bar{\sigma}}(k\bar{r})e^{i\kappa x}d\bar{r} + \int_S [g(\bar{r})-1]\bar{\bar{\sigma}}(k\bar{r})e^{i\kappa x}d\bar{r}\right)\bar{\bar{T}}\bar{\mathbf{a}}_E \\ &= e^{i\kappa x_l}\left(\bar{\bar{\mathbf{I}}}_1 + \bar{\bar{\mathbf{I}}}_2\right)\bar{\bar{\mathbf{T}}}\bar{\mathbf{a}}_E\end{aligned} \tag{6}$$

where S is the positive half-space excluding the area occupied by the lth particle. To evaluate $\bar{\bar{\mathbf{I}}}_1$ and $\bar{\bar{\mathbf{I}}}_2$, we use the Hankel function addition theorem [1]

$$\left[\bar{\bar{\sigma}}(k\overline{r_j r_l})\right]_{nm} = H_{m-n}^{(1)}(k|\overline{r_j r_l}|)e^{i(m-n)\phi_{jl}} \tag{7}$$

where $\overline{r_j r_l}$ is the translation vector between coordinate systems, ϕ_{jl} is the angle that the vector makes with the x-axis, and m and n denote the harmonics in the jth and the lth coordinate systems, respectively.

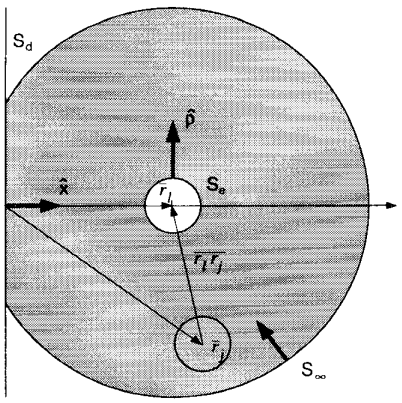

Fig. 1. Domain of integration. Shown are the three surfaces (S_d, S_e, and S_∞) and their inward pointing surface normals for the integral in (18).

To solve the integral $\bar{\bar{\mathbf{I}}}_1$, we note that $y_p = H_p^{(1)}(k\rho)e^{-ip\phi}$ is a solution to the wave equation, as is $e^{i\kappa x}$. By applying Green's second identity to the combination of the two wave equations consisting of these solutions, $\bar{\bar{\mathbf{I}}}_1$ becomes a contour integral

$$\left[\bar{\bar{\mathbf{I}}}_1\right]_{nm} = \frac{n_0}{\kappa^2 - k^2}\int_C \left[e^{i\kappa x}\nabla y_p - y_p \nabla e^{i\kappa x}\right]\cdot d\bar{C} \tag{8}$$

(where $p = n - m$), as shown in Fig. 1. $\bar{\bar{\mathbf{I}}}_1$ may be written in terms of the three components of the surface

$$\bar{\bar{\mathbf{I}}}_1 = \frac{-n_0}{\kappa^2 - k^2}\left(\bar{\bar{\mathbf{I}}}_e + \bar{\bar{\mathbf{I}}}_d + \bar{\bar{\mathbf{I}}}_\infty\right) \tag{9}$$

where inward pointing normals were used for convenience. By employing the far-field condition, $\bar{\bar{\mathbf{I}}}_\infty = 0$, we are left with an integration over the exclusion disc, $\bar{\bar{\mathbf{I}}}_e$ and the half space surface, $\bar{\bar{\mathbf{I}}}_d$. Explicitly, the integral $\bar{\bar{\mathbf{I}}}_e$ may be written as

$$\left[\bar{\bar{\mathbf{I}}}_e\right]_{nm} = k\rho H_p^{'(1)}(k\rho)Y_p - \rho H_p^{(1)}(k\rho)\frac{\partial}{\partial\rho}Y_p \tag{10}$$

where

$$Y_p = -\int_{-\pi}^{\pi} e^{-ip\phi}e^{i\kappa\rho\cos\phi}d\phi = 2\pi i^p J_p(\kappa\rho). \tag{11}$$

Substituting (11) into (10) and evaluating at $\rho = b$ we have

$$\left[\bar{\bar{\mathbf{I}}}_e\right]_{nm} = 2\pi i^p\left[kbH_p^{'(1)}(kb)J_p(\kappa b) - \kappa b H_p^{(1)}(kb)J_p'(\kappa b)\right]. \tag{12}$$

The surface integral $\bar{\bar{\mathbf{I}}}_d$ over the planer surface $x = -x_l$ is

$$\left[\bar{\bar{\mathbf{I}}}_d\right]_{nm} = e^{i\kappa x}\frac{\partial}{\partial x}X_p - i\kappa e^{i\kappa x}X_p \tag{13}$$

where

$$X_p = \int_{-\infty}^{\infty} H_p^{(1)}(k\rho)e^{-ip\phi}dy = \frac{-2}{k}e^{ik|x|}. \tag{14}$$

Substituting (14) into (13) and evaluating at $x = -x_l$ gives

$$\left[\bar{\bar{\mathbf{I}}}_d\right]_{nm} = 2ie^{i(k-\kappa)x_l}\left[1 + \frac{\kappa}{k}\right]. \tag{15}$$

For the second integral in (6), we have

$$\left[\bar{\bar{\mathbf{I}}}_2\right]_{nm} = n_0\int_{\substack{\rho>b\\ x>-x_l}} [g(\bar{r}) - 1]H_p^{(1)}(k\rho)e^{-ip\phi}e^{i\kappa x}d\bar{r} \tag{16}$$

where we note that $\bar{\bar{\mathbf{I}}}_2$ is dependent on the propagation constant κ, the pair distribution function $g(\bar{r})$, the particle diameter, and the particle location x_l. If we notice, however, that $[g(\bar{r}) - 1]$ is nearly zero for $|\bar{r}|$ greater than a few particle diameters, we can treat the integration as if it were over an unbounded space, thus ignoring the boundary at $x = -x_l$ (and particles near that boundary)

$$\left[\bar{\bar{\mathbf{I}}}_2\right]_{nm} = n_0\int_{-\pi}^{\pi}\int_b^{\infty}[g(\bar{r}) - 1]H_p^{(1)} \times (k\rho)e^{-ip\phi}e^{i\kappa\rho\cos\phi}\rho\, d\rho d\phi. \tag{17}$$

Furthermore, if we assume that the pair distribution function is axially symmetric, (17) may be written as a single integral which can be calculated numerically

$$\left[\bar{\bar{\mathbf{I}}}_2\right]_{nm} = 2\pi n_0 i^p\int_b^{\infty}[g(\rho) - 1]H_p^{(1)}(k\rho)J_p(\kappa\rho)\rho\, d\rho. \tag{18}$$

Depending on the particular problem, the appropriate form of $\bar{\bar{\mathbf{I}}}_2$ given by (16), (17), or (18) may be used.

Referring back to (6), we can multiply $\bar{\bar{\mathbf{I}}}_1$ and $\bar{\bar{\mathbf{I}}}_2$ by $e^{i\kappa x_l}$ to get a new expression

$$\bar{\bar{\mathbf{s}}} = \left[\bar{\bar{\mathbf{s}}}_1 e^{i\kappa x_l} + \bar{\bar{\mathbf{s}}}_2 e^{ikx_l}\right]\bar{\bar{\mathbf{T}}}\bar{\mathbf{a}}_E \tag{19}$$

where the explicit dependence of (6) on the constant of propagation (k or κ) has been made clear. In (19) we have

$$\bar{\bar{\mathbf{s}}}_1 = \frac{-n_0}{\kappa^2 - k^2}\bar{\bar{\mathbf{I}}}_e + \bar{\bar{\mathbf{I}}}_2 \tag{20}$$

and

$$\bar{\bar{\mathbf{s}}}_2 = \frac{2in_0 k}{\kappa - k}. \tag{21}$$

Using (19) in (5), the multiple scattering equation may be written

$$\bar{\mathbf{a}}_E e^{i\kappa x_l} = \left[\bar{\bar{\mathbf{s}}}_1 e^{i\kappa x_l} + \bar{\bar{\mathbf{s}}}_2 e^{ikx_l}\right]\bar{\bar{\mathbf{T}}}\bar{\mathbf{a}}_E + e^{ikx_l}\bar{\mathbf{a}}_{\text{inc}}. \tag{22}$$

If we balance the exponential terms of e^{ikx_l} and $e^{i\kappa x_l}$, we then have two independent equations

$$0 = \bar{\bar{\mathbf{s}}}_2\bar{\bar{\mathbf{T}}}\bar{\mathbf{a}}_E + \bar{\mathbf{a}}_{\text{inc}} \tag{23}$$

$$\bar{\mathbf{a}}_E = \bar{\bar{\mathbf{s}}}_1\bar{\bar{\mathbf{T}}}\bar{\mathbf{a}}_E \tag{24}$$

which comprise the Ewald–Oseen extinction theorem (23) and the Lorentz–Lorenz law (24). To find the constant of propagation, we solve (24) by noticing that the determinant of the matrix

$$\bar{\bar{\mathbf{Q}}} = \left[\bar{\bar{\mathbf{s}}}_1\bar{\bar{\mathbf{T}}} - \bar{\bar{\mathbf{I}}}\right] \tag{25}$$

must be equal to zero for the nontrivial solution. Thus, the solution for QCA rests in minimizing the determinant of a matrix whose elements are related to $\bar{\bar{\mathbf{s}}}_1$ and the single particle

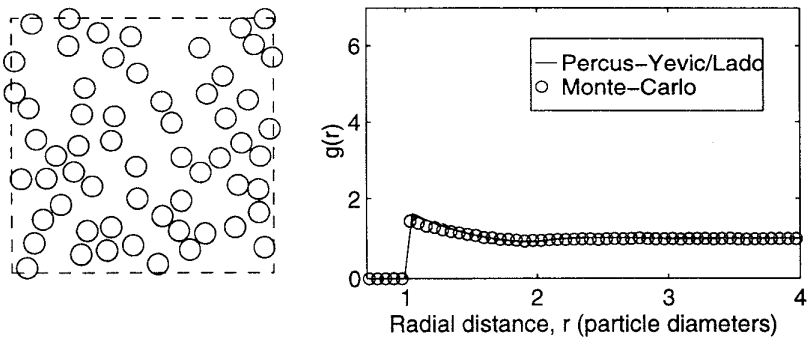

Fig. 2. Simulation of a classical fluid for a volume fraction of 30%. Shown are results from Monte-Carlo numerical simulations and the PY equation in two dimensions solved by Lado.

transition matrix, $\bar{\bar{\mathbf{T}}}$. Only the transition matrix in (25) is dependent on the field polarization. For a circularly symmetric cylinder, the T-matrix is diagonal and is given by [8]

$$T_{mm}^{\mathrm{TM}} = \frac{-k_i J_m(ka) J_m'(k_i a) + k J_m'(ka) J_m(k_i a)}{k_i H_m^{(1)}(ka) J_m'(k_i a) - k H_m^{'(1)}(ka) J_m(k_i a)} \delta_m \quad (26)$$

for the TM polarization and

$$T_{mm}^{\mathrm{TE}} = \frac{-k_i/\epsilon_i J_m(ka) J_m'(k_i a) + k/\epsilon_0 J_m'(ka) J_m(k_i a)}{k_i/\epsilon_i H_m^{(1)}(ka) J_m'(k_i a) - k/\epsilon_0 H_m^{'(1)}(ka) J_m(k_i a)} \delta_m \quad (27)$$

for TE polarization. In (26) and (27), k_i and ϵ_i indicate the propagation constant and permittivity of the inclusions. The factor δ_m is equal to unity for $m = 0$ and two for $m \geq 1$.

Thus, to implement QCA, the matrix $\bar{\bar{\mathbf{Q}}}$ is constructed from either of (26) or (27) from above and (20), $\bar{\bar{\mathbf{s}}}_1$ which employs (12), $\bar{\bar{\mathbf{I}}}_e$, and (18), $\bar{\bar{\mathbf{I}}}_2$. The effective constant of propagation of the random medium is

$$\kappa_{\mathrm{eff}} = \min_{\kappa} [\det \bar{\bar{\mathbf{Q}}}]. \quad (28)$$

The user defined variables in (28) are: 1) the pair distribution function, $g(\bar{r})$, 2) the particle density, n_0, 3) the particle diameter, b, and 4) the maximum order of the cylindrical wave expansion, $p_{\max}$ such that $p \in [0, p_{\max}]$. From a practical point of view, the pair distribution function is the most difficult of these variables to determine.

As a basis of comparison, we may use the single scattering field approach of the effective field approximation (EFA) also known as Foldy's approximation. In two dimensions, the effective permittivity for circular inclusions determined by EFA is

$$\epsilon_{\mathrm{eff}} = 1 - n_0 \frac{4i}{k^2} \sum_m T_{mm}^{\mathrm{TM\ or\ TE}}. \quad (29)$$

III. Pair Distribution Function

In the previous section, we developed the theory for the 2-D quasi-crystalline approximation. After developing the theory it was noted that the pair distribution function was the unknown which was most difficult to characterize. In reality the pair may be estimated in one of three ways: 1) experimentally, 2) theoretically, or 3) numerically. Experimental estimation of the pair is extremely difficult due to the fact that it entails a detailed study of the particle structure for each random medium being considered. A theoretical approach may be used to model the physical distribution of particles in a medium but we may be limited to only a certain class of media which may be described by the mathematical model. Alternatively, a numerical approach may be used to directly model the arrangements of particles via Monte Carlo simulations based on a computer model the particle deposition. The numerical model, has the advantage of increased flexibility in addressing a variety of physical methods of particle deposition and interaction.

We present here a set of four distinct pair distribution functions, each has been given a simple label (in parentheses) that will be used for reference in the remainder of the paper.

Hole Correction (HC): The hole correction formula is the simplest of the theoretical pair distribution functions and can be used to model an ideal gas consisting of monosized particles of diameter b

$$g(\rho) = \begin{cases} 0 & \rho < b \\ 1 & \rho \geq b \end{cases} \quad (30)$$

HC has the effect of eliminating the $\bar{\bar{\mathbf{I}}}_2$ term in (20) and, thus, it is possible to use QCA-HC as a measure to gauge the effect of the pair distribution function on the QCA formulation.

Classical Fluid Medium (PY): Of the theoretical pair distribution functions, the most common is given by Percus and Yevick [1958] which can be used to model particle positions in a classical fluid of hard spheres. 3-D closed-form solutions of PY can be found in Wertheim [1963] and have been shown to agree closely with numerical simulations of particle arrangements [2]. In two dimensions, the PY equations have been solved numerically by Lado [1968] (Fig. 2). The assumptions of hard-sphere PY are 1) there are no external forces acting on the particles and 2) the potential energy between particles is infinite when they overlap and zero when their centers are separated by a distance greater than one particle diameter. The first assumption allows the system energy to be directly related to the particle arrangement and the second assumption creates a basis from which this energy may be calculated. These assumptions are the physical parallel of placing particles randomly within a confining volume until a given volume fraction or particle density has been reached.

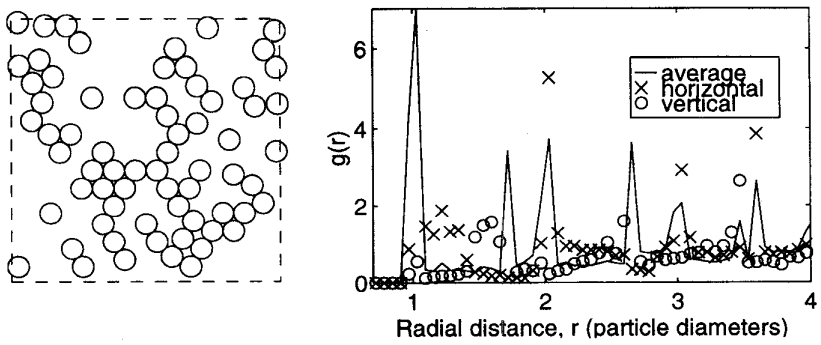

Fig. 3. Particle arrangement simulation using particle extraction from a near perfect lattice for a volume fraction of 30%. Shown is the average pair distribution function over all angles and the pair distribution function from the vertical and horizontal directions which accentuate the azimuthal asymmetry. Because the basic structure of the lattice remains unchanged for different volume fractions, the pair distribution function does not change with particle number density.

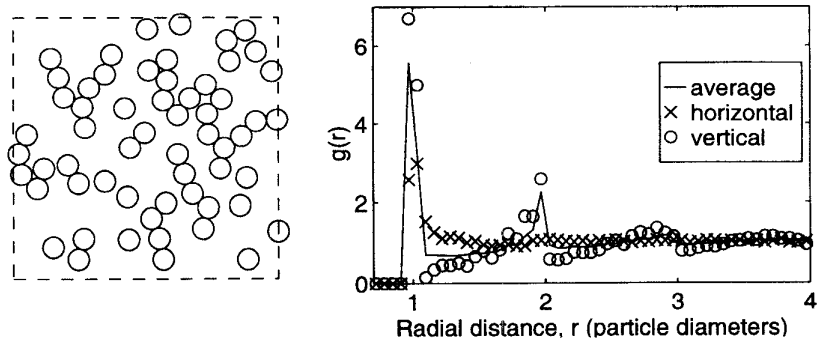

Fig. 4. Simulation of a 2-D snow-type medium for a volume fraction of 30%. Shown is the average pair distribution function over all angles and the pair distribution function from the vertical and horizontal directions which accentuate the azimuthal asymmetry.

In performing 2-D numerical simulations, it was found that volume fractions from zero to approximately 48% were attainable without resorting to arrangement initialization techniques (such as given by Metropolis *et al.* [5]). Initialization techniques allow high particle densities to be reached by initializing particle positions to a totally packed crystalline array. Individual realizations are performed by perturbing particles from their original positions by a random vector. It should be noted that by resorting to this method, we can no longer guarantee an axially symmetric pair distribution function and for this reason, only volume fractions below 45% are generally used for the analysis component of this paper. It may be, however, that it is possible to determine a mean pair distribution function which calculates probable particle locations based on radial distance only and ignores the angular dependence by averaging over all angles. While this violates the assumption made in determining (18), we can examine the effects of the approximation here.

Particle Extraction Method (Extract): Particles are arranged together in a near crystalline fashion using a packing algorithm (PA) described in Siqueira *et al.* [10]. Particles are removed one by one without disturbing the lattice until the desired volume fraction is achieved (Fig. 3). Because of the effect of gravity, the pair distribution function is not axially symmetric. The pair distribution function is shown in the vertical direction ($\circ$), the horizontal direction ($\times$), and for the azimuthal average (solid line).

Snow-Type Medium (Snow): This 2-D simulation utilizes PA to simulate the process of falling snow (Fig. 4). In this simulation, deposited particles are made to stick near their initial starting points after which the volume fraction is adjusted using the extraction method. Particles are not allowed to find their state of minimum potential energy. This stacking process is reflected in the pair distribution function which illustrates an ordered array in the vertical direction ($\circ$) and a disordered one in the horizontal direction ($\times$).

In this section, we have discussed four different methods of arranging particles in a volume or area. Each of the different methods were presented to illustrate the variety of pair distribution functions that can be achieved by altering the method of particle deposition in the simulations. The presentation accentuated the fact that the pair distribution functions are not necessarily axially symmetric nor similar, effects that will be further explored in the paper. The resulting pair distribution functions can be used directly in the QCA theory developed in the previous section to analyze the sensitivity of QCA to the pair distribution function $g(\bar{r})$ or we can extend our evaluation one step farther by using the particle position simulations to directly determine the effective constant of propagations for a random medium.

IV. Independent Determination of ϵ_{eff}

This section provides a brief review of a numerical method (NUM) of determining the effective permittivity of a 2-D

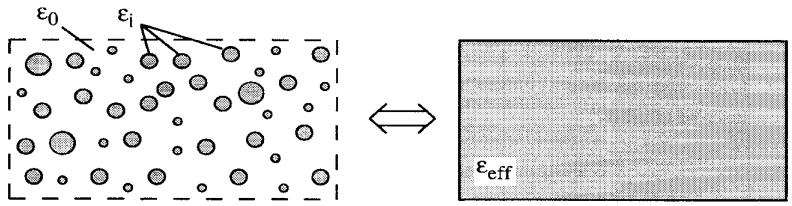

Fig. 5. Model for numerical determining ϵ_{eff} for a random medium.

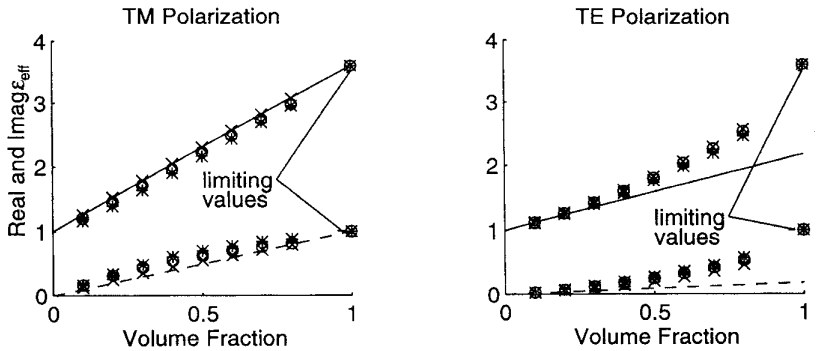

Fig. 6. Effective permittivity ϵ_{eff} versus volume fraction for a TM-polarized field incident upon a random medium. Shown are results from the numerical method for different particle sizes along with those obtained by the Polder-Van Santen mixing formula [9]. The volume fraction was adjusted by particle extraction.

random medium [9]. Given a method of arranging particles in a volume, it is possible to directly determine ϵ_{eff} using a numerical solution to Maxwell's equations. In the paper describing this method, it has been shown that the technique agrees well with the low-frequency mixing formula of Polder and Van Santen [1956] when dielectric losses are more significant than scattering losses. This method has also been demonstrated to show appropriate behavior in the low-frequency region as well as for both sparse and very dense concentrations of particles.

The numerical method compares the average scattered field from a random collection of particles confined within an imaginary boundary with that of a homogeneous dielectric body whose shape is the same as the imaginary boundary (Fig. 5). By varying the permittivity of the homogeneous body, we may minimize the difference between the scattered fields of the two bodies. One such example is given in Fig. 6 for both the TM and TE polarizations for three different particle sizes using the particle extraction method of adjusting volume fraction. Shown also in the figures is the 2-D PVS mixing formula given by

$$\epsilon_{\text{eff}} = \epsilon_h + f(\epsilon_i - \epsilon_h) \tag{31}$$

$$\epsilon_{\text{eff}} = \epsilon_h + f(\epsilon_i - \epsilon_h)\frac{2}{\epsilon_i + \epsilon_h} \tag{32}$$

for the TM and TE polarizations, respectively. It can be seen that for the small particle sizes that there is excellent agreement between the two methods at low-volume fractions. Furthermore, the increased losses shown for larger particles is consistent with physical expectations. What remains to be done is to include results from the 2-D QCA theory developed in Section II and to compare those results with the results from this section for the four different methods of generating particle arrangements (HC, PY, extract, and snow).

V. Evaluation of the Two-Dimensional Quasi-Crystalline Approximation

In this section, the behavior of QCA as a function of particle size, polarization, volume fraction, scattering/dielectric losses and particle arrangement method is explored. To begin, we present three sets of six plots (Figs. 7–9) which demonstrate the theoretical and numerical methods dependence on particle size, volume fraction, polarization, and dielectric loss. Fig. 7 (TM polarization) and Fig. 8 (TE polarization) demonstrate real and imaginary ϵ_{eff} performance for particles with a modest amount of dielectric loss ($\epsilon_i = 3.6 + i0.1$), while Fig. 9 gives the imaginary component of ϵ_{eff} for particles with low dielectric loss ($\epsilon_i = 3.6 + i0.01$) for both TM and TE polarizations. The real component of ϵ_{eff} is not included in Fig. 9 because it was found that the behavior of $\text{Re}(\epsilon_{\text{eff}})$ did not change appreciably from the examples given in Figs. 7 and 8. In all three figures, a classical fluid (PY) was used to model particle positions for both QCA and the numerical method. The particle diameters used in each of the demonstrations range from $\lambda_i/10(kd = 0.33)$, $2\lambda_i/10$ $(kd = 0.67)$ to $3\lambda_i/10$ $(kd = 1.0)$ as the plots go from left to right (k is the wavenumber of the included particles).

Referring to Figs. 7–9, the following observations are in order.

$\text{Re}(\epsilon_{\text{eff}})$ *TM Polarization:* The real part of the effective permittivity is practically the same for the theoretical methods of PVS, EFA, QCA-PY, QCA-HC, and NUM-PY for all volume fractions, particle size, and both values of particle

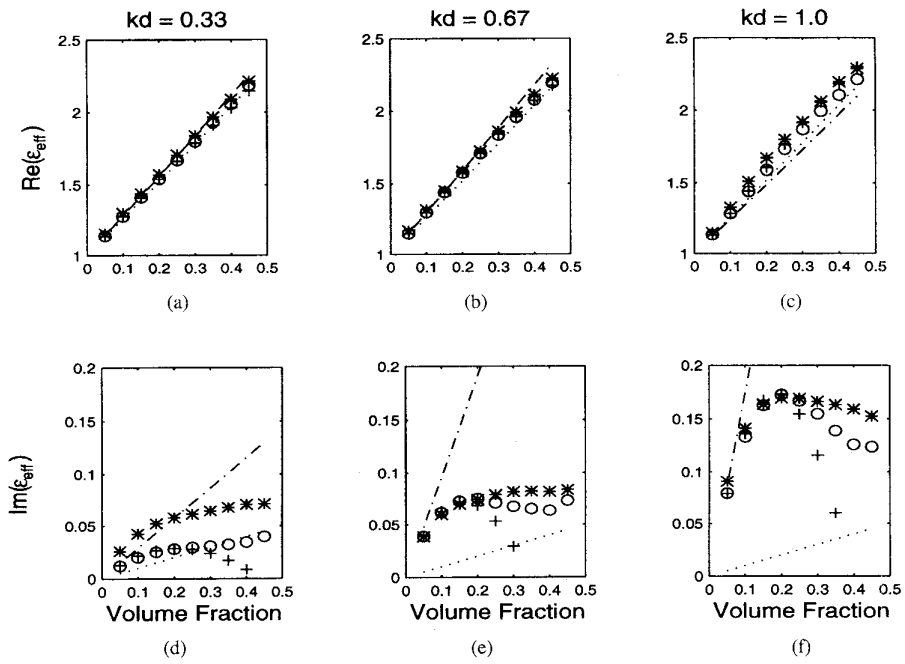

Fig. 7. Comparison between five methods of determining effective permittivity for a TM polarized field: EFA (−.), PVS (···), QCA-PY(o), QCA-HC (+) and NUM-PY (∗). Plots (a)–(c) illustrate $\mathrm{Re}(\epsilon_{\mathrm{eff}})$, and (d)–(e) illustrate $\mathrm{Im}(\epsilon_{\mathrm{eff}})$ as a function of volume fraction using a model of particles ($\epsilon_i = 3.6 + i0.1$) suspended in a classical fluid. Particle diameter ranges from $\lambda_i/10$ ($kd = 0.33$) [(a) and (d)], $2\lambda_i/10$ ($kd = 0.67$) [(b) and (e)], to $3\lambda_i/10$ ($kd = 1.0$) [(c) and (f)].

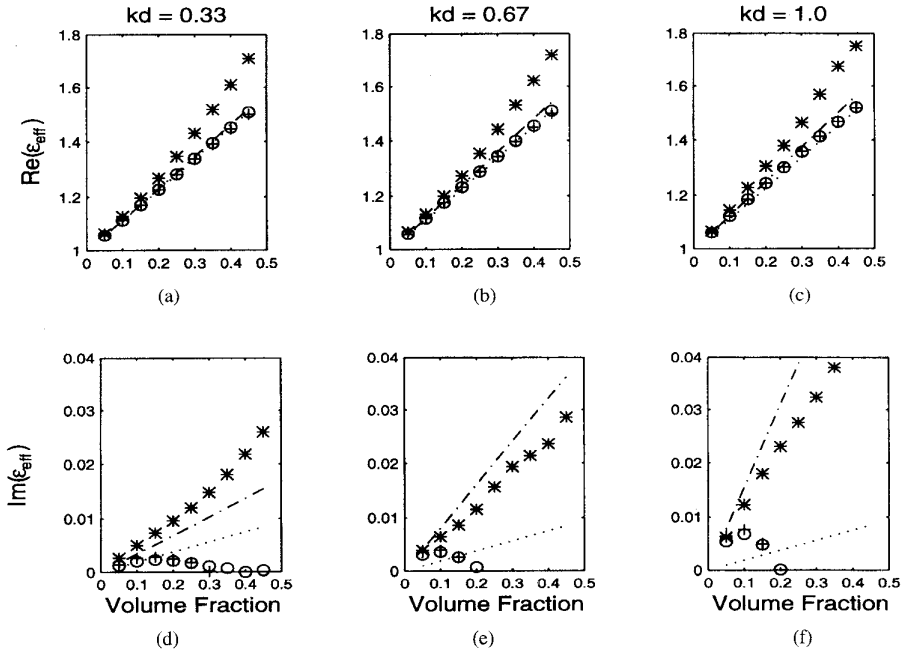

Fig. 8. Comparison between five methods (QCA-PY, QCA-HC, EFA, PVS and NUM-PY) of determining effective permittivity for a TE-polarized field (see caption of Fig. 7 for details).

dielectric loss [Fig. 7(a)–(c)]. The performance of EFA and PVS degrades as particle size increases, an effect of an increase in scattering by the larger particles. Both QCA-PY and QCA-HC track the behavior of the numerical method well in this aspect because of the inclusion of multiple scattering terms in the QCA formulation. Note that PVS may be used as a reference as particle size varies because particle size is, in general, not a factor in mixing formulas. Therefore, we may notice, via PVS, that QCA-PY, QCA-HC, and NUM-PY agree that phase velocity decreases with increasing particle size. The similarities between the results of $\mathrm{Re}(\epsilon_{\mathrm{eff}})$ for both low-loss and moderate-loss inclusions indicate that dielectric loss in the

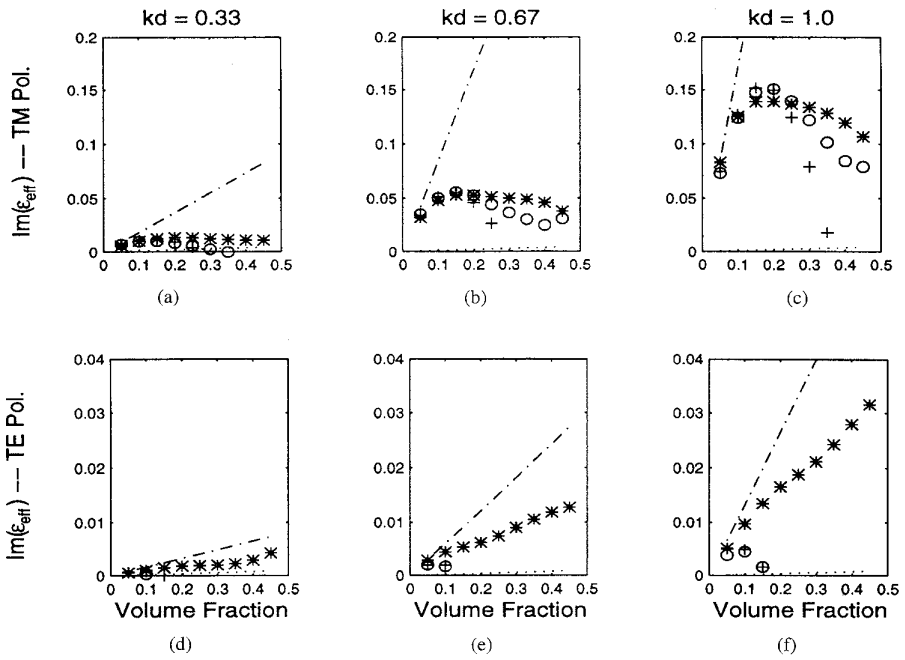

Fig. 9. Comparison between five methods (QCA-PY, QCA-HC, EFA, PVS, and NUM-PY) of determining the effective permittivity for TM- and TE-polarized fields. The permittivity of the included particles is $\epsilon_i = 3.6 + i0.01$. The real component (not shown) is essentially unchanged from the previous example when $\epsilon_i = 3.6 + i0.1$. See the caption in Fig. 7 for details.

particles does not appreciably effect the phase velocity. This may also highlight the effect that only near particle interactions effect the real part of ϵ_{eff}.

$\text{Im}(\epsilon_{\text{eff}})$, *TM Polarization:* The imaginary part of the effective permittivity displays a more complex behavior than the real part as a function of volume fraction and particle size. The theoretical and numerical methods agree well at low-volume fractions with the exception of small particle sizes for moderately lossy inclusions [Fig. 7(d)]. In this respect, while it is known in the low-frequency limit that all the methods agree, the losses indicated by NUM-PY are significantly larger than results given by the theoretical methods of QCA-HC and QCA-PY. We believe that these differences may be caused by an overestimation of absorption losses with respect to the multiple scattering losses for the methods of QCA-PY and QCA-HC. That is, numerically, we detect more multiple scattering than QCA does for moderately lossy particles with sizes that are relatively small with respect to wavelength.

We may also note that QCA-PY does an excellent job of tracking the losses predicted by NUM-PY for the larger particle sizes shown in Fig. 7(e) and (f). At a volume fraction of approximately 20% the methods of QCA-PY and QCA-HC diverge significantly with a trend reversal seen in QCA-PY due to the contribution from the pair distribution function. In both cases, for the larger particles we also see a significant difference between EFA, QCA-PY, QCA-HC, NUM-PY, and that of PVS, an effect that is expected because of the scattering losses incurred by the larger particles are not accounted for by the mixing formula.

The change in $\text{Im}(\epsilon_{\text{eff}})$ is considerably more noticeable between Fig. 7(d)–(f) and Fig. 9(a)–(c). Proportional to the PVS mixing formula, the losses are significantly larger for $\epsilon_i = 3.6 + i0.01$ than for $\epsilon_i = 3.6 + 0.1$, indicating that multiple scattering is a much more dominant factor in the low loss case. The multiple scattering however does not translate into greater losses overall as we can see that the numerical method predicts lower losses, in general, than the losses predicted for particles with higher dielectric loss. What this means is that although the field in the $\epsilon_i = 3.6 + i0.01$ case interacts with more particles, the field does not suffer enough additional absorption losses due to the multiple interactions to make up for the absorption losses incurred with the lossier $\epsilon_i = 3.6 + i0.1$ particles. We also make a final note that QCA does a comparably well job at predicting $\text{Im}(\epsilon_{\text{eff}})$ in this case, as it did in the previous TM case when $\epsilon_i = 3.6 + i0.1$.

$\text{Re}(\epsilon_{\text{eff}})$ *TE Polarization:* The real parts of ϵ_{eff} for all methods and particle sizes agree well at the low-volume fractions but begin to deviate at a volume fraction of about 20% [Fig. 8(a)–(c)]. This effect is expected because of the necessary nonlinear contribution from electrical dipoles to the total field for the TE polarization. The trends of EFA, QCA-PY, and QCA-HC all follow that of the PVS model relatively well despite an even poorer performance for the theoretical methods in the prediction of scattering losses (discussed below). We note that NUM displays the physically expected trend of ϵ_{eff} approaching ϵ_i as volume fraction increases toward unity.

$\text{Im}(\epsilon_{\text{eff}})$ *TE Polarization:* We may first note that all methods agree well, with respect to losses, at very low-volume fractions irrespective of particle size. In the 0%–20% volume fraction range it is evident that QCA-PY and QCA-HC reflect the correct trend of increased scattering loss for increased particle size. However, for this polarization, the dominant term

in (20) is $\bar{\bar{\mathbf{I}}}_e$ (the particle exclusion integral) and not $\bar{\bar{\mathbf{I}}}_2$ (the integral dependent on the pair distribution function). Thus, $\mathrm{Im}(\epsilon_{\mathrm{eff}})$ becomes unphysically negative as can be seen through the effect of QCA-PY following QCA-HC into the nonphysical domain of negative $\mathrm{Im}(\epsilon_{\mathrm{eff}})$. QCA-PY and QCA-HC do not adequately describe the multiple scattering losses at fractional volumes greater than 5% and, in fact, the scattering losses under-predicted by QCA-PY and QCA-HC significantly fall below the lower limit given by the PVS mixing formula.

In Fig. 9(d)–(f) we illustrate the behavior of $\mathrm{Im}(\epsilon_{\mathrm{eff}})$ for low-loss particles whose permittivity is $\epsilon_i = 3.6 + i0.01$. Without the additional support of dielectric losses, QCA gives realistic values for $\mathrm{Im}(\epsilon_{\mathrm{eff}})$ for only the smallest of volume fractions. As with the TM case, the losses predicted by NUM-PY are larger in proportion to the losses predicted by PVS but are smaller overall than the losses shown in Fig. 8(d)–(f).

It may be disturbing to see the poor performance of QCA in its ability to predict losses for TE-polarized fields (Figs. 8 and 9). To answer questions related to this effect, it is useful to examine the low frequency behavior of QCA (or more specifically QCA-HC) for both the TM and TE polarizations (Fig. 10). Only the hole correction formula with QCA is used in this demonstration to examine the effect of the exclusion integral, $\bar{\bar{\mathbf{I}}}_e$, term in (20). The results of QCA-HC are compared with the PVS mixing formula (which is essentially the low-frequency limit of EFA) so that a single curve can be used as a reference for different particle sizes. The real component of ϵ_{eff} for both polarizations follows that of PVS very closely for all particle sizes and, therefore, is not shown. Only for particle diameters of $\lambda_i/20$ and larger does $\mathrm{Im}(\epsilon_{\mathrm{eff}})$ deviate significantly from PVS for the two polarizations, but the deviation for the TM polarization is much milder than that shown for a TE-polarized field in which ϵ_{eff} actually becomes negative. We attribute these differences to the higher order singularity found in the Green's function for a TE polarized field (i.e., dipole interactions instead of monopole interactions as is the case for TM polarization). The negative trend seen for the TE-polarized field is much more difficult for the $\bar{\bar{\mathbf{I}}}_2$ term in (20) to overcome and it is for this reason that we see the degraded performance of the TE-polarization results shown in Figs. 8 and 9.

Given the extensive analysis presented so far with respect to the performance of QCA, EFA, PVS, and NUM, it is convenient to present the results in a more compact form. To this end, we present Fig. 11 which graphically illustrates the differences between the three theoretical method's (QCA, EFA, and PVS) and the numerical method's (NUM) estimation of ϵ_{eff} in terms of validity regions. The differences used to determine the validity regions were computed in terms of errors with respect to the numerical method given by

$$\mathrm{err} = \frac{\mathrm{theory} - \mathrm{NUM}}{\mathrm{NUM}} \times 100\%. \tag{33}$$

The numerical method is used as a reference because there are no current exact formulations to determine ϵ_{eff} in the regions under consideration and the numerical method is the only method presented thus far that displays the expected

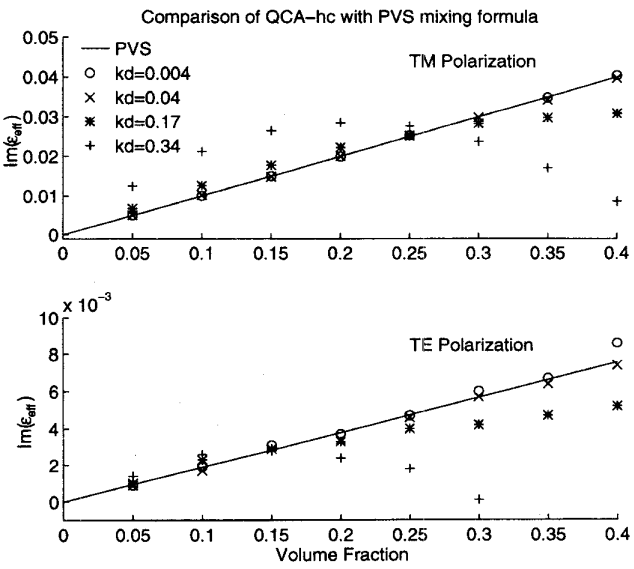

Fig. 10. Performance of QCA-HC at very low frequencies. Shown is $\mathrm{Im}(\epsilon_{\mathrm{eff}})$ for particles with diameter $\lambda_i/800$, $\lambda_i/80$, $\lambda_i/20$, and $\lambda_i/10$ for both TM and TE polarizations ($\epsilon_i = 3.6 + i0.1$).

behavior of ϵ_{eff} as a function of volume fraction, particle size, and polarization. The validity regions were drawn to enclose areas where differences between the numerical and theoretical methods were less than 20%. The validity regions shown are based on a grid of numerical simulations that varied the volume fraction from 5%–45% in 5% steps and varied particle sizes from $kd = 0.33$ to $kd = 1.0$ in steps of one third. It should be noted that because NUM is used as a reference, errors in NUM will manifest themselves as a systematic offset in the presented validity regions of QCA, EFA, and PVS. Additional regions of validity have also been drawn for the limiting cases of low-frequency and low-fractional volume where all of the different methods employed are known to converge. Because of computational limitations, it was not possible to test the high-frequency limits of the theoretical methods.

Fig. 11 illustrates well the behavior of the theoretical methods as a function of volume fraction, particle size and polarization. QCA-PY for the TM polarization does well with the exception of $kd = 0.33$-sized particles (a region which was discussed earlier) and the region of volume fractions extending between 30% and 40%. In this latter region, the reduced performance of QCA is most likely due to an enhanced component of multiple scattering with respect to the other volume fractions. This behavior has been observed both numerically and experimentally [6].

As a final analysis of QCA, we compare the numerical method's evaluation of ϵ_{eff} with that of QCA for the array of different particle arrangement methods presented earlier (Fig. 12). To simplify the treatment, only the angular averaged pair distribution functions were used. At a volume fraction of 30% and $\epsilon_i = 3.6 + 0.01$ we expect multiple scattering to play an important role in determining ϵ_{eff}. It can be noticed that the exact form of the pair distribution function has little effect on

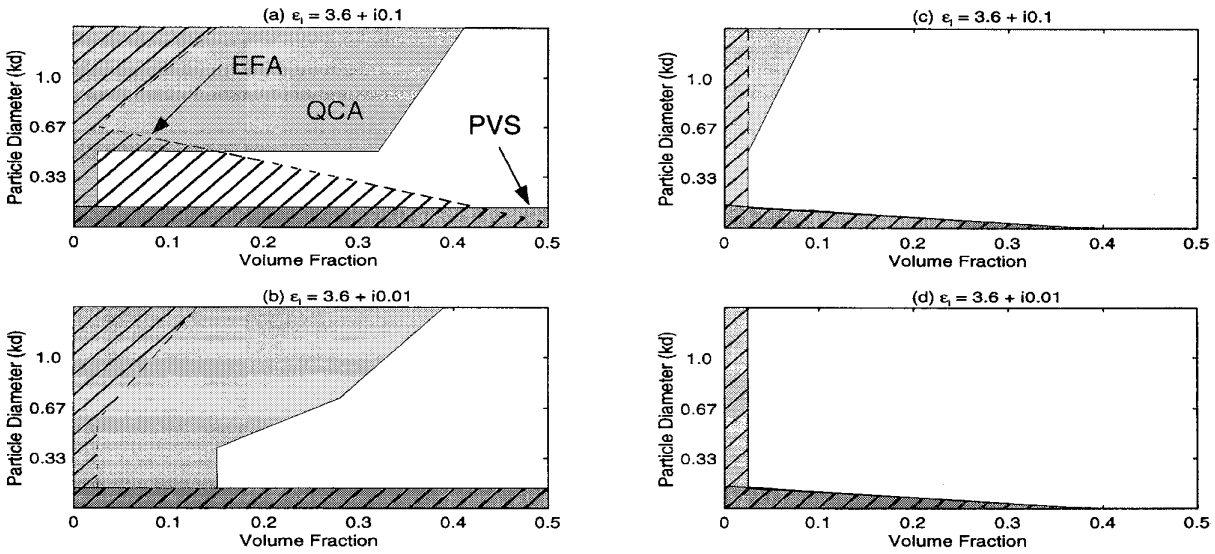

Fig. 11. Validity regions based on 20% differences between imaginary ϵ_{eff} for the numerical method of determining ϵ_{eff} (NUM-PY) and the theoretical methods of QCA-PY (light gray), EFA (hatched) and PVS (dark gray) for (a) TM, $\epsilon_i = 3.6 + i0.1$, (b) TM, $\epsilon_i = 3.6 + i0.01$, (c) TE, $\epsilon_i = 3.6 + i0.1$, (d) TE, $\epsilon_i = 3.6 + i0.01$. The plain white regions indicate where none of the theoretical models yield satisfactory results.

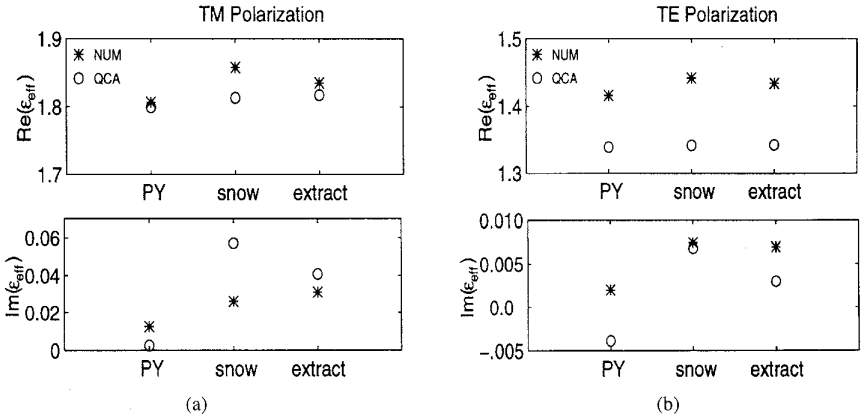

Fig. 12. Effective permittivity comparison between particle arrangement methods. Volume fraction = 30%, $\epsilon_i = 3.6 + i0.01$, (a) TM polarization and (b) TE polarization.

the performance of QCA or NUM for $\text{Re}(\epsilon_{\text{eff}})$ for both the TM and TE polarizations, with the possible exception of the snow simulation.

More interesting however is the behavior of $\text{Im}(\epsilon_{\text{eff}})$ to the different methods of particle arrangement. By examining Figs. 2–4, it can be seen that the PY simulation yields a loose collection of scatterers whereas the extraction technique generally yields sets of compact groups. The snow-type medium simulation falls somewhere between these two extremes. The enhancement of scattering losses when particles are clumped together is reflected in the results given by NUM; $\text{Im}(\epsilon_{\text{eff}})$ is least for PY and greatest for the extraction method. Physically, this makes sense, the grouping together of particles acts as a coherent collection of scatterers whose cross section is greater than what it would be for all of the scatterers acting independently. The implications of this result argues strongly against the use of the Percus–Yevick pair distribution function (which models a classic fluid) in the determination of extinction for granular media deposited under the influence of gravity. Snow, sand, and soils are good examples of the type of media which fall into this category.

VI. Conclusion

In this paper, we have made a complete analysis of the subject of determining effective permittivity for dense random media in two dimensions. The popular method of the quasi-crystalline approximation was derived and associated results for the effective field approximation and the mixing formula for both TM and TE polarizations were presented. Because QCA depends on the form of pair distribution function used, a variety of different particle arrangement methods were presented. We then discussed a numerical method based on the method of moments which may also be used to determine

effective permittivity and has been shown to follow expected trends from low to high density and from low to high frequency. The behavior of the methods and the general behavior of effective permittivity were then studied for a variety of different situations, from which it was possible to determine regions of validity for the theoretical methods based on the presented numerical method. Finally, a comparison was made between the effective permittivities found by the numerical method and the quasi-crystalline approximation as a function of particle arrangement method. From this analysis, we have made the following conclusions.

1) The real component of effective permittivity is essentially the same for all methods up to a value of $kd \approx 1$. The TM polarization, in this respect, is valid for all volume fractions and the TE polarization is valid up to a volume fraction of 20%.
2) Given 20% error bounds, the losses predicted by QCA for the TM polarization agree quite well with the numerical method [Fig. 11(a) and (b)]. It is important however to use the correct form of pair distribution function [Fig. 12(a)].
3) The losses predicted by QCA for the TE polarization agree very poorly with the numerical method [Fig. 11(c) and (d)]. At volume fractions greater than 15% it is not uncommon for $\mathrm{Im}(\epsilon_{\mathrm{eff}})$ to become unphysically negative. We believe this poor behavior is due to the strong singularity found in the Green's function for this polarization.
4) The effect of decreasing absorption losses of the inclusions has the expected effect of increasing multiple scattering but this does not translate into higher total losses.
5) The pair distribution function (or similarly, the particle arrangement method) does play an important role in determining extinction (Fig. 12). It is believed that this is due to the effect of two neighboring particles acting together as a single larger particle. Thus, it is inappropriate to use the Percus–Yevick pair distribution when analyzing a random medium whose particle locations do not resemble a classical fluid.

The work presented in the paper opens up a number of avenues for future work. In two dimensions, the effect of the angular asymmetry in the pair distribution function on QCA can be explored by carrying out the 2-D integration in (17). It would also be informative to analyze the effect of varying $\mathrm{Re}(\epsilon_i)$ on ϵ_{eff} and to determine an empirical method of determining the effective permittivity based on a combination of QCA and generalized results found by NUM. The most important and useful future work, however, will be to bring the presented analysis and methods into three dimensions. In this sense, the study presented here offers an important set of methods and background that can be used to conduct that investigation.

REFERENCES

[1] W. C. Chew, Y. M. Wang, and L. Gurel, "Recursive algorithm for wave-scattering solutions using windowed addition theorem," *J. Electromagn. Waves Applicat.*, vol. 6, no. 11, pp. 1537–1560, Nov. 1992.

[2] K. H. Ding, C. E. Mandt, L. Tsang, and J. A. Kong, "Monte Carlo simulations of pair distribution functions of dense discrete random media with multiple sizes of particles," *J. Electromagn. Waves Applicat.*, vol. 6, no. 8, pp. 1015–1030, Aug. 1992.

[3] C. C. Lu, W. C. Chew, and L. Tsang, "The application of recursive aggregate T-matrix algorithm in the Monte Carlo simulations of the extinction rate of random distribution of particles," *Radio Sci.*, vol. 30, no. 1, pp. 25–28, Jan./Feb. 1995.

[4] C. E. Mandt, Y. Kuga, L. Tsang, and A. Ishimaru, "Microwave propagation and scattering in a dense distribution of nontenuous spheres: Experiment and theory," *Waves Random Media*, vol. 2, pp 225–234, 1992.

[5] N. Metropolis, A. W. Rosenbluth, M. N. Rosenbluth, and A. H. Teller, "Equation of state calculations by fast computing machines," *J. Chem. Phys.*, vol. 21, no. 6, pp. 1087–1092, June 1953.

[6] A. Nashashibi and K. Sarabandi, "A technique for measuring the effective propagation constant of dense random media," presented at *IEEE AP-S Int. Symp.*, Newport Beach, CA, June 1995.

[7] D. Polder and J. H. VanSanten, "The effective permeability of mixtures of solids," *Physica*, vol. 12, no. 5, pp. 1257–271. Aug. 1946.

[8] G. T. Ruck, D. E. Barrick, W. D. Stuart, and C. K. Krichbaum, *Radar Cross-Section Handbook*. New York: McGraw-Hill, 1970.

[9] K. Sarabandi and P. R. Siqueira, "Numerical scattering analysis for two-dimensional dense random media: Characterization of effective permittivity," *IEEE- Trans. Antennas Propagat.*, to be published.

[10] P. R. Siqueira, K. Sarabandi, and F. T. Ulaby, "Numerical simulation of scatterer positions in a very dense media with an application to the two-dimensional born approximation," *Radio Sci.*, vol. 30, no. 5, pp. 1325–1339, Sept./Oct. 1995.

[11] H. Stark and J. M. Woods, *Probability, Random Processes, and Estimation Theory for Engineers*. Englewood Cliffs, NJ: Prentice-Hall, 1986.

[12] L. Tsang, C. E. Mandt, and K. H. Ding, "Monte Carlo simulations of the extinction rate of dense media with randomly distributed dielectric spheres based on solution of Maxwell's equations," *Opt. Lett.*, vol. 17, no. 5, Mar. 1992.

[13] L. Tsang, J. Kong, and R. Shin, *Theory of Microwave Remote Sensing*. New York: Wiley, 1985.

Paul Siqueira was born in Skokie, IL, on June 27, 1966. He received the B.S. and M.S. degrees in electrical engineering from Iowa State University, Ames, in 1987 and 1990, respectively. He is currently a Ph.D. candidate at the University of Michigan, Ann Arbor, in the Radiation Laboratory.

From 1990 to 1991, he worked as an image processing consultant to the University of Chicago, Chicago, IL, in the Department of Astronomy and Molecular Biology. His research interests are in inhomogeneous wave propagation, microwave sensor development, and signal and image processing for remote sensing applications.

Kamal Sarabandi (S'87–M'90–SM'93), for photograph and biography, see p. 266 of the February 1996 issue of this TRANSACTIONS.